Toyota Mirai: powertrain model and assessment of the energy management

Mauro Carignano and Ramon Costa-Castelló,

***Abstract*—Toyota Mirai is a widely known fuel cell hybrid vehicle and its powertrain represents a benchmark for engineers and researchers. This work presents a lumped-parameter low-order model of Toyota Mirai powertrain and an assessment of the energy management focused on fuel economy and battery and fuel cell degradation. In addition, a rule-based strategy is proposed to reproduce the behavior of Toyota Mirai energy management strategy. The powertrain model and the proposed strategy are validated against experimental data. The assessment of the energy management is performed by comparing the Toyota Mirai strategy with optimal strategies obtained offline via dynamic programming. Different optimal strategies are computed by including the demand of the fuel cell and the battery in the cost function. Simulation results show a high correlation between the proposed model and strategy compared to the experimental data. Comparison of Toyota Mirai strategy with the optimal strategies reveals a small margin for improvement in fuel economy and higher margins in terms of demand of the fuel cell and battery.**

***Index Terms*—Keywords: Hybrid vehicle, Fuel cell vehicle, Energy management, Optimal strategy, Toyota Mirai**

I. Introduction

Fuel Cell Hybrid Vehicles (FCHV) represents an alternative with great potential to deal with pollution problems associated with land transport. Among the best known FCHV are Toyota Mirai, Honda Clarit, Hyundai Tucson and Nexo, Chevrolet Equinox and Volkswagen Passat Lingyu. Despite the promising results in terms of energy efficiency and operational emissions, this technology still has some aspects that need to be improved to make this technology more affordable and profitable. These aspects are related to lifespan and cost of the components and to the storage, distribution and production of hydrogen (H_2). A comprehensive review of the current challenges for H_2-based technologies and FCHV is presented in [1].

Fuel Cells (FC) offer zero emission during vehicle operation and a higher efficiency compared to internal combustion engines. However, FC present some limitations such as idle periods and slow-transient response. Due to the latter the FC must be operated with certain restrictions to avoid premature degradation. Evidence shows that certain damage mechanisms in FC are promoted by fast power variations [2]–[4].

Energy Management Strategy (EMS) in FCHV has an impact both on the H_2 consumption and lifetime of the power sources. Generally, lower fuel consumption in FCHV comes at the expense of high demand on power sources and vice versa. As a consequence, the EMS faces a trade-off between fuel economy and the care of power sources. An example of this trade-off is presented in [5]. Although fuel consumption accounts for the largest percentage of all costs over the lifetime of a hybrid vehicle [6], premature degradation of power sources could lead to early component replacement which is undesirable and should be minimized. The replacement of components such as the FC or the battery represents a significant percentage of the total cost and emissions of the vehicle [7].

Toyota began the development of FC systems in 1992. In 2014, after more than 20 years of R&D, they launched the Toyota Mirai first generation, Japan's first mass-produced FCHV. In this way, Toyota became a pioneer in FCHV and Toyota Mirai powertrain represents a benchmark for engineers and researchers. Although many articles present detailed descriptions about Toyota Mirai technology [8]–[11], to the best of our knowledge, none of them so far presented a comprehensive study of its energy management or a simple model to perform powertrain system level simulations. As for energy management, this work aims to reveal the margin for improvement currently available.

This paper presents i) a lumped-parameter low-order model of the powertrain used in Toyota Mirai first generation, ii) an assessment of the energy management focused on both fuel economy and battery and FC degradation, and iii) a rule-based strategy that aims to reproduce the behavior of the Toyota Mirai energy management strategy. The proposed model and strategy are parameterized and validated using experimental data from a chassis dynamometer in a controlled laboratory environment [12]. The assessment of the energy management is complemented by comparing Toyota Mirai against optimal strategies computed offline via dynamic programming.

Next, Section II describes the Toyota Mirai and presents the mathematical models, Section III analyzes the Toyota Mirai EMS and presents the proposed rule-based strategy. Finally, simulation results and conclusions are presented in Section IV and V, respectively.

II. Powertrain Model and Experimental Data

An overview of the Toyota Mirai first generation and a schematic representation of the powertrain are shown in Fig.1. Detailed information about technological aspects can be found in [8]–[11].

The powertrain model proposed in this work is a power-flow oriented low-order non-linear model. It focuses on component

Mauro Carignano is with Capgemini Engineering Belgium. E-mail: mauroguido.carignano@capgemini.com

Ramon Costa-Castelló is with Universitat Politècnica de Catalunya (UPC). E-mail: ramon.costa@upc.edu.

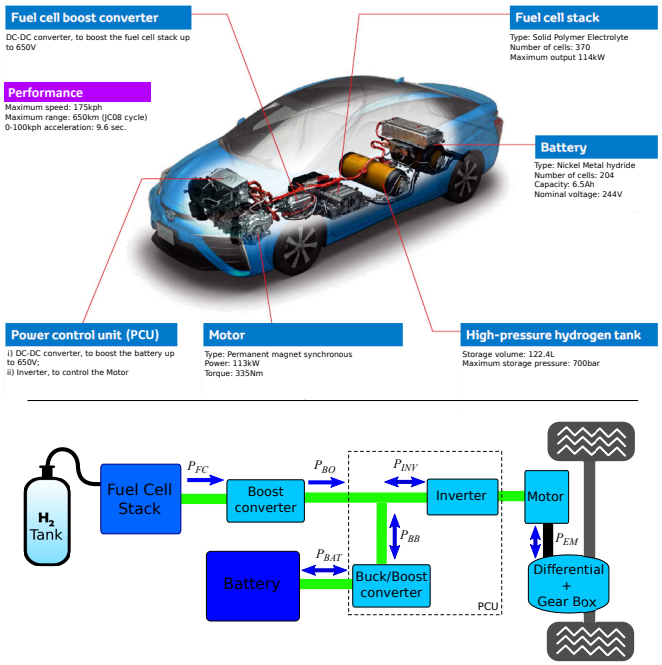

Figure 1. Upper: Toyota Mirai first generation overview (image from [13]). Lower: powertrain schematic.

efficiencies and neglects fast dynamics. In the following sections the experimental data is described and the models of the powertrain components are presented.

A. Experimental Data

This work uses data obtained from real tests conducted by Argonne National Laboratory [12]. This data is from the Downloadable Dynamometer Database and was generated at the Advanced Mobility Technology Laboratory (AMTL) at Argonne National Laboratory under the funding and guidance of the U.S. Department of Energy (DOE). On a chassis dynamometer under a controlled environment, the laboratory performed multiple tests of Toyota Mirai (model year 2017). Results include different driving cycles at different temperatures. The data collected during these tests and a technical report are available free-of-charge in the laboratory website [14]. Data includes measurements from original CAN channels and sensors added by the laboratory. All experimental data is available at a sampling rate of 10Hz.

The tests listed in Table I were used to calibrate and validate the models presented in this work. These tests were performed at room temperature (22 °C). The first six tests are called Set 1 and were used for parametrization, while the last two tests were used for validation and analysis.

B. Battery model

The dynamic behavior of the battery is reproduced by a model presented by Tremblay [15] and Cabello [16]. In this model, the battery voltage at time k is given by,

$$U_{BAT}(k) = U_{BAT,oc}(k) - R_{BAT}\ I_{BAT}(k), \qquad (1)$$

Table I
LIST OF TESTS USED IN THIS WORK. SET 1: ABOVE DASHED LINE

Test ID [14]	Cycle
61712010	UDDS
61712045	WLTP
61712012	HWFET
61712042	JC08
61712043	NEDC
61712018	US06
61712053	UDDS
61712046	WLTP

where $U_{BAT,oc}$ is the open-circuit voltage, I_{BAT} is the current and R_{BAT} is the internal resistance. Then, $U_{BAT,oc}$ depends on the filtered current (I^*_{BAT}) and on the battery state of charge (SOC) as follows:

$$U_{BAT,oc}(k) = U_{BAT,0} - K_1(1 - SOC(k)) - K_2\ I^*_{BAT}(k), \qquad (2)$$

where $U_{BAT,0}$, K_1 and K_2 are tuning parameters. The SOC dynamics is calculated as follows [17],

$$SOC(k+1) = SOC(k) - \frac{I_{BAT}(k)\ \eta^{sign(I_{BAT}(k))}\ t_s}{Q_{BAT,0}}, \qquad (3)$$

where η is the coulomb efficiency, $Q_{BAT,0}$ the battery capacity and t_s the time step. Note that the current is considered negative for charging and positive for discharging. The battery current is computed from the power demand (P_{BAT}),

$$I_{BAT}(k) = \frac{U_{BAT,oc}(k) - (U^2_{BAT,oc}(k) - 4P_{BAT}(k)R_{BAT})^{0.5}}{2\ R_{BAT}}. \qquad (4)$$

and the filtered current I^*_{BAT} through a low-pass first-order filter,

$$I^*_{BAT}(k) = \frac{I^*_{BAT}(k-1)\ \tau_{BAT} + I_{BAT}(k)\ t_s}{\tau_{BAT} + t_s}, \qquad (5)$$

where τ_{BAT} is a tuning parameter known as battery time constant.

Toyota Mirai battery is composed of 204 Nikel-Metal Hydride cells connected in series. From the experimental data it was observed that this battery is able to deliver/receive a maximum power of 30kW. Each cell has a capacity of $6\,Ah$ ($Q_{BAT,0}$) and $1.2\,V$ of nominal voltage. The rest of the parameters are obtained using the experimental data. First, $U_{BAT,0}$ and K_1 are computed using the open-circuit voltages in steady conditions for different $SOCs$. Then, with current and voltage profiles in transient conditions, K_2, τ_{BAT} and R_{BAT} were calculated using the least squares criterion. In the available experiments, the vehicle operates most of the time with SOC between 50% to 65%, and therefore the tuning focuses on this range.

The following parameters were obtained using data from UDDS cycle (test ID 61712053): $U_{BAT,0} = 316.7\,V$, $K_1 = 101\,V$, $R_{BAT} = 0.3629\,\Omega$, $K_2 = 0.4458\,\Omega$, $\tau_{BAT} = 40\,s$ and $\eta = 0.98$. Fig. 2 compares the battery voltage and the SOC reproduced by the model with the measured values. The voltage differences between the measurement and the model are presented on the right of the Fig. 2. This histogram shows that in 99 % of the computed values, the voltage difference

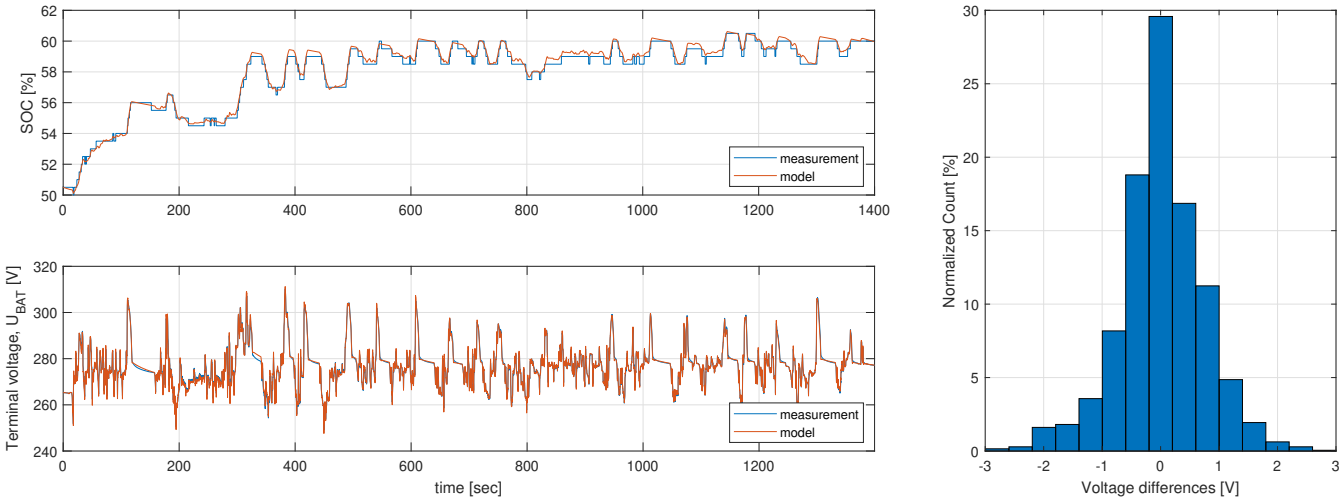

Figure 2. Left side: Behavior of battery voltage under dynamic conditions, comparison measurements vs. model. Right side: Histogram of voltage differences between measurement and model. Measurements and inputs for simulation are taken from Test ID 61712053 (UDDS cycle), Table I.

between measurement and model is lower than $2\,V$. The model with these parameters was validated using experimental data from WLTP cycle (test ID 61712046) and the results are presented in Fig. 3. As can be seen, the differences between the model and measurements in terms of SOC and voltage are as low as in the UDDS cycle (Fig. 2).

C. Battery aging

For the purpose of this work it is useful to estimate the battery degradation under dynamic conditions. This section describes the model used to estimate battery lifetime from a given current profile. The model uses the concept of *Ah-throughput*, stating that the battery reaches its end of life after a certain amount of charge circulates through it [18]–[21]. Variables such as discharge/charge rate (C_{rate}), Depth of Discharge (DOD) and operating temperature are considered by this model.

The index C_{rate} is the ratio between the current I_{BAT} in Amperes and the nominal capacity of the battery Q_{BAT} in Ah:

$$C_{rate} = \frac{|I_{BAT}|}{Q_{BAT}}. \tag{6}$$

C_{rate} is used by battery manufacturers to express the speed of discharge or charge of the battery. In battery data sheets, the information regarding lifespan refers to durability tests normally performed with C_{rate} equals or lower than 1.

In this aging model, the effective *Ah-throughput* for a given current profile is computed as follows,

$$Ah_{eff}(t) = \int_0^t |I_{BAT}(\tau)|\ \sigma(\tau)\ d\tau, \tag{7}$$

where σ is a variable named severity factor that depends on the DOD, battery temperature and C_{rate}. The severity factor increases when the C_{rate} and DOD increase and is always greater than 1. Operating temperatures above certain limits also increase the severity factor value. The maximum C_{rate} computed from the experimental data (cycles UDDS and WLTP) was $14\,h^{-1}$ which corresponds to a severity factor of 2 according to [22]. As will be seen in the results, the SOC varies in a narrow strip (between 50 % and 65 %), and therefore the dependency of σ on the DOD can be neglected. The effect of the DOD is relevant when the SOC shows deep charge/discharge cycles, as in the case of battery electric vehicles. Finally, the battery temperature observed from the experimental data is relatively low and shows small variations (between 32 °C and 36 °C). In this condition, the effect of the temperature has a low impact in this model and therefore is neglected. According to the previous statements, for this application the severity factor only depends on the C_{rate} and is calculated as described in [22].

Once the effective *Ah-throughput* is computed, the fraction of battery life consumed is estimated as:

$$BAT_{life}(t) = \frac{Ah_{eff}(t)}{Ah_{nom}}. \tag{8}$$

The degradation is cumulative and the battery reaches its end of life when BAT_{life} equals 1. Therefore, minimizing the Ah_{eff} extends the battery lifetime. The degradation model described in this section was used for NiMH and Li-ion batteries in [20], [21] and [18], [19], respectively.

D. Fuel Cell Model

The Toyota Mirai is equipped with a proton exchange membrane (PEM) FC composed by 370 cells, able to reach a maximum power of $114\,kW$. Detailed information about the development of this FC can be found in [11]. The FC model required for this work consists of a quasistatic model capable of calculating H_2 consumption as a function of FC power. The FC performance of Toyota Mirai in different driving cycles and the fitting proposed are shown in Figure 4. Note that in all figures the plotted values were calculated using original data provided by Argonne National Laboratory. Part of the

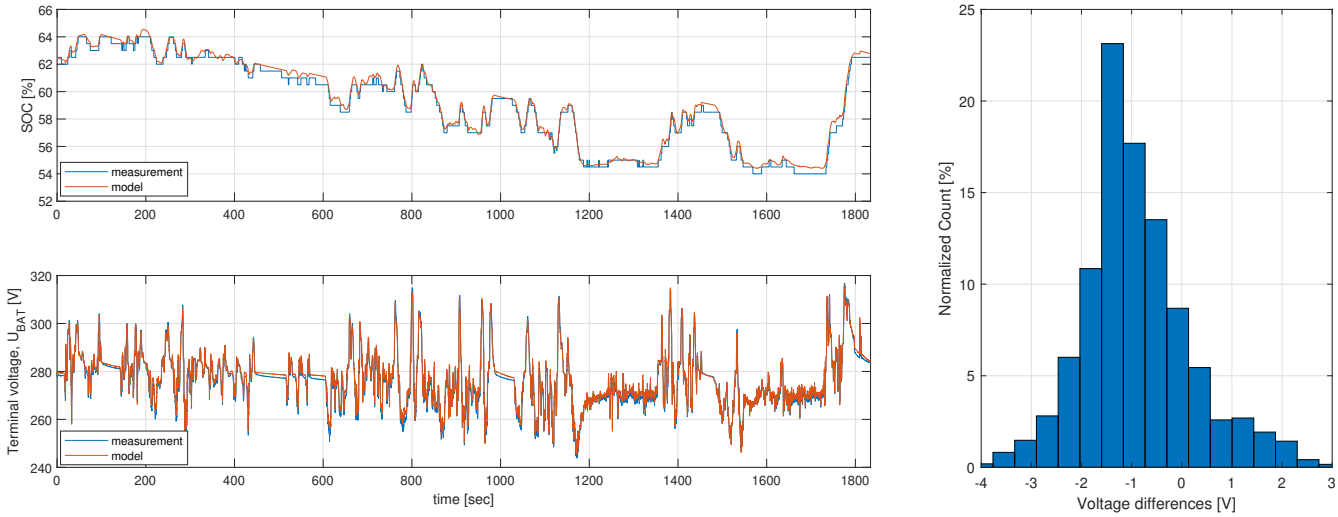

Figure 3. Left side: Behavior of battery voltage under dynamic conditions, comparison measurements vs. model. Right side: Histogram of voltage differences between measurement and model. Measurements and inputs for simulation are taken from Test ID 61712046 (WLTP cycle), Table I.

dispersion observed in the figures presented in this section may be related to measurement and synchronization errors of the experimental data.

In Figure 4-b the behavior of current versus power shows a low scatter of points around a quadratic fit. This means that the FC current can be obtained as a function of FC power using an algebraic equation.The maximum power demand of the FC in UDDS and WTLC cycles is below 55kW and only in cycle US06 the FC power demand exceeds 55kW. On the other hand, the maximum power demand of the motor in UDDS and WTLC cycles is also below 55kW. Then, the fitting proposed for the FC is up to 80kW, providing a power range wide enough to cover the simulations of this work.

A curve fitting for the FC voltage is presented in Figure 4-a. The first part of the expression in 4-a represents the open circuit voltage and the second part the voltage drop due to the internal resistance. The parameters $A = 0.0474$ and $N = 370$ are known constants, while $I0 = 40.91\ A$, $E0 = 0.9759\ V$ and $R1 = 0.05317\ \Omega$ were fitted from experimental data. As can be seen, the expression proposed fits well up to $350\ A$. Below $20\ A$ (idle phase), Toyota Mirai FC system is starved of hydrogen to maintain a low open-circuit voltage [12], and therefore this zone was excluded from the fitting.

The instantaneous H_2 consumption is proportional to the current [23]:

$$\dot{m}_{H_2} = \frac{0.03761}{3600}\ N_{cell}\ I_{FC,gross}\ , \tag{9}$$

where $I_{FC,gross}$ is the stack current (i.e. gross current) in amperes, $\dot{m}_{H_2}$ is the hydrogen mass flow rate in grams per second and N_{cell} is the number of cells in the FC stack. This expression considers only the H_2 that reacts in the stack. The H_2 released by purges also contributes to the total consumption but to a lesser extent. Furthermore, the amount of H_2 released in purges is hard to estimate with a model and no related experimental data is available to compute it. After comparing the H_2 consumption reported with that computed with formula 9, it can be stated that the H_2 consumed by purges is negligible compared to the H_2 used in the chemical reaction. It was reported in [12] that the FC consumes $4.39\ g/hr$ of H_2 during idle to maintain the low open circuit voltage.

The stack efficiency is the ratio between the gross power delivered by the FC and power from the H_2 consumed. The latter is obtained by multiplying the instantaneous H_2 consumption (9) by the H_2 specific energy ($120\,MJ/Kg$). The stack efficiency reaches a maximum of around 66% at 10kW. To compute the system efficiency shown in Figure 4-c, the consumption of FC auxiliary components (water and H_2 pumps and air compressor) is included. Figure 5 shows the total consumption of auxiliary components as a function of the FC gross power.

It is worth mentioning that models based on curve fittings are usually used to estimate hydrogen consumption in vehicle powertrain applications. Models used in [24]–[26] are examples of the previous statement. More complex and precise models can be found in the literature but are not suitable for optimal control applications. Additionally, specific experimental data is necessary to calibrate models with higher complexity. The chosen model must be adjusted to problem needs and energy management algorithms rarely use higher complexity models.

Regarding the limitations to operate the FC, the variation of the output power (power rate) is considered. As it was mentioned, fast power variations contribute to FC degradation. A wide range of criteria can be found in the literature about the FC power rate constraints. Some authors adopt conservative values around 2% of its maximum power per second [27], [28], while higher values, between 5% and 40%, were adopted by [24], [26], [29]–[33]. Other authors as [34]–[37] do not consider any limitation for the FC power rate. From the experimental data it was observed that Toyota Mirai can reach

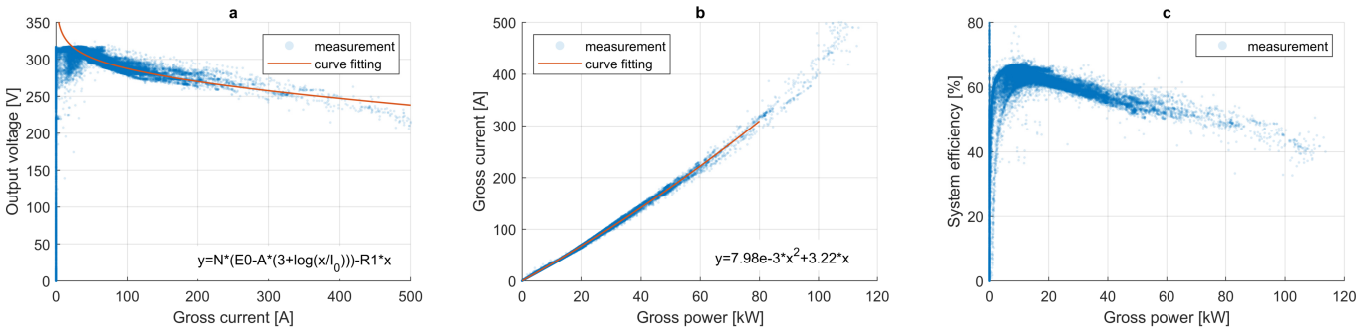

Figure 4. Fuel cell performance and proposed fitting (experimental data from Set 1, Table I).

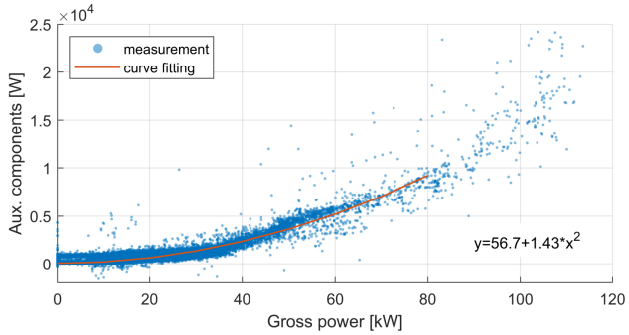

Figure 5. Power consumption of FC auxiliary components and proposed fitting (experimental data from Set 1, Table I)

a maximum FC power variation of $100\,kW$ per second for rising and falling, i.e. power rate of 88%.

The power variation in the FC is defined as:

$$\Delta P_{FC}(k) = \frac{P_{FC}(k) - P_{FC}(k-1)}{t_s}, \tag{10}$$

where $P_{FC}(k)$ is the FC power at time k. This variable is called control input and is computed by the EMS, as will be shown later. The control input $P_{FC}(k)$ is constrained as follows:

$$0 \leq P_{FC}(k) \leq 114, \tag{11}$$

$$-100 \leq \Delta P_{FC}(k) \leq 100. \tag{12}$$

where P_{FC} and ΔP_{FC} are in kW and kW/s, respectively. Notice that (12) depends on the current and the previous power value in the FC. This leads to the need to use the instantaneous FC power as a state variable, with its state equation:

$$x_{FC}(k+1) = P_{FC}(k). \tag{13}$$

As a consequence, (12) is a state-dependent constraint.

Finally, to evaluate the demand of the FC aimed at its degradation, the following two phenomena are considered [38]:

- Fast power variations ($\overline{\Delta P}_{FC}$), computed as the average of the power gradient for ΔP_{FC} greater than $10\,kW/s$;
- Idle time ($\%t_{idle}$), computed as the percentage of time that the FC is idle compared to the total cycle time.

E. Power Electronic Converters and Motor

These components are considered in the powertrain model through their efficiencies, which are computed via algebraic expressions.

1) Boost Converter: this converter boosts the voltage from the FC output to the DC-BUS and controls the power flow between them. The DC-BUS voltage varies between 320 and $650\,V$, while the voltage at the FC terminals varies between 220 and $317\,V$. The boost converter can handle input and output currents up to $500\,A$ and $165\,A$, respectively. Detailed information about the development of this converter can be found in [39]. Figure 6 shows its performance and the proposed model.

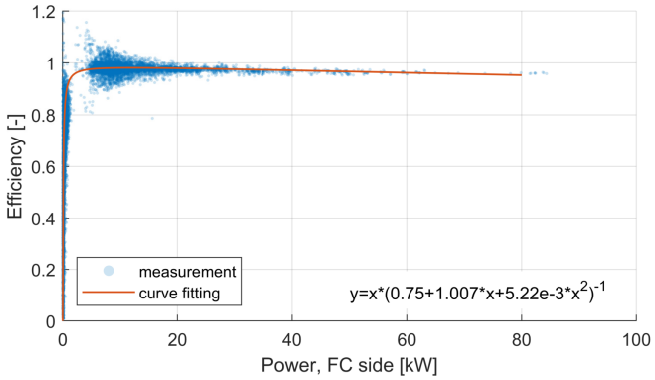

Figure 6. Boost converter performance and proposed fitting (experimental data from Set 1, Table I)

The dispersion in this case leads to efficiencies greater than 1, which is certainly not possible. However, the negative impact of such dispersion in our fitting is minimized by the fact that this dispersion is symmetric, i.e. there are efficiencies greater than 1 as well as very low efficiencies for the same FC power. As in the case of the FC, part of the dispersion observed in the figures presented in this section may be related to measurement and synchronization errors of the experimental data.

2) Buck/Boost Converter: this converter controls the power flow between the battery and the DC-BUS. Battery voltage varies between 225 and $320\,V$. The buck/boost converter can handle battery side currents up to $150\,A$. Unfortunately, for this

converter there is no experimental data available on the DC-BUS side. There is a condition where it is possible to compute the buck/boost converter efficiency using the experimental data. This is when the power consumed/delivered by the motor is null. In this way, the power input in the Buck/Boost converter (working as Buck) is the power output of the Boost converter (available in the experimental data). As only a reduced number of points meet this condition, it is hard to fit a curve. Instead, a constant average efficiency is adopted, obtained by integrating the power values at both sides of the converter and computing the ratio. Using the experimental data from Set 1, the efficiency is 97.8%. This efficiency will also be used when the converter works as a Boost.

3) Motor and Inverter: the inverter is connected to the DC-BUS and to the motor. There is no experimental data available from the inverter on the DC-BUS side nor on the motor side. As an alternative, it is proposed i) to model these components together (motor + inverter) and ii) consider the points where the battery power flow is null, in such a way the electrical power entering the inverter is equal to the boost converter power -available in the experimental data- (see Figure 1). Figure 7 shows the combined performance of these components and the proposed curve fitting. The fitting goes up to 60kW, providing a power range wide enough to cover the simulations of this work.

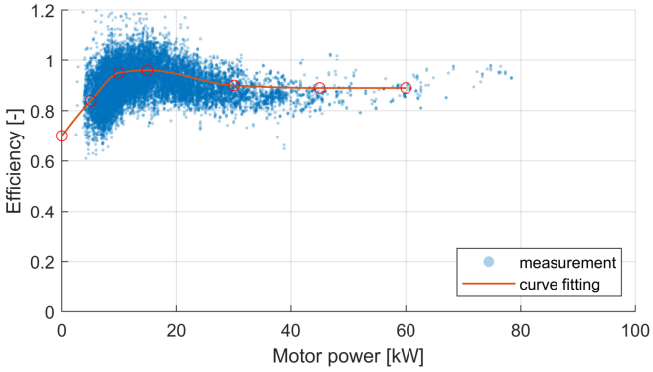

Figure 7. Motor and Inverter combined performance and proposed fitting (experimental data from Set 1, Table I)

The fitting proposed is a cubic interpolation using the following vectors as input data:
$x = [0, 5, 10, 15, 30, 45, 60]$;
$y = [0.7, 0.84, 0.95, 0.96, 0.9, 0.89, 0.89]$,
where x is the mechanical power in the motor (in kW). To reduce the observed dispersion, the authors evaluated the possibility of using torque and motor revolutions instead of power as inputs, but the results obtained did not show any improvement.

F. FCHV model

Fig. 8 shows a schematic representation of the proposed Toyota Mirai powertrain model. It is the result of integrating the models presented in the previous sections. Causality is indicated by red arrows and power flows by blue arrows. $P_{FC}(k)$ is the control input and a variable computed by

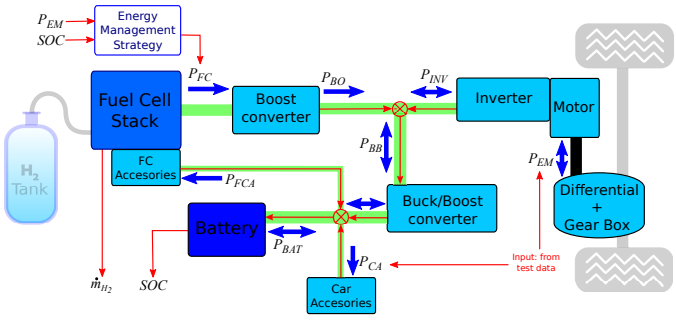

Figure 8. Schematic representation of the proposed model

the EMS. The power in the electric motor $P_{EM}(k)$ depends on the power at the driving wheels. $P_{EM}(k)$ is considered an input and is obtained from the experimental data. Car accessories include the heater and car electric accessories (connected to $12\,V$ battery). Car accessories power P_{CA} takes constant values of $462\,W$ and $489\,W$ for UDDS and WLTP cycles, respectively. These values were obtained averaging the consumptions available from the experimental data (Test ID 61712053 and 61712046, Table I).

III. Energy Management

In this section, the EMS of Toyota Mirai is analyzed from experimental data and a rule-based strategy is proposed to reproduce its behavior. Additionally, the formulation of the global optimization problem is presented to obtain three optimal EMS via Dynamic Programming.

A. Rule-based strategy

The strategy presented in this section aims to replicate the behavior of Toyota Mirai EMS. The intention is not to mimic the original EMS of Toyota Mirai but to achieve a performance similar to that observed from the experimental data. Based on the experience of the authors of this article, and after post-processing and analyzing the experimental data in different driving cycles, the following can be stated:

- The FC operates in two main conditions: i) Idle: no power delivery; and ii) Active: power delivery following the power demand on the motor.
- When the FC is active, the minimum power delivered is around $7\,kW$.
- The battery SOC operates between 50 % and 65 % in normal conditions and 55 % is the average value observed.

Fig. 9 shows how the FC transitions from idle to active and vice versa. P_{on} and P_{idle} are thresholds that depend on the SOC, as shown in Fig. 10.

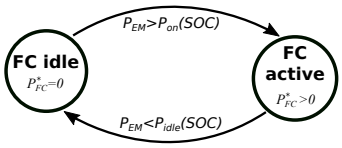

Figure 9. FC operating conditions and transitions

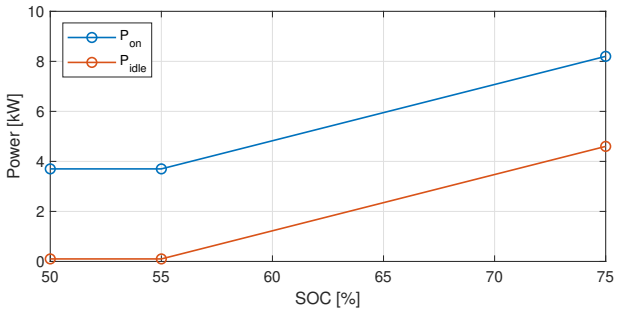

Figure 10. Thresholds for FC transitions. SOC and P_{EM} are X and Y axis inputs respectively

When the FC is active, P^*_{FC} is computed as function of P_{EM} and SOC as follows:

$$P^*_{FC}(P_{EM}, SOC) = \begin{cases} P_{low}(P_{EM}) & \text{if } SOC > 55.25, \\ P_{mid}(P_{EM}) & \text{if } 54.75 < SOC < 55.25, \\ P_{hi}(P_{EM}) & \text{if } SOC < 54.75, \end{cases} \tag{14}$$

where P_{hi} and P_{low} are mapped as shown Fig. 11. Then, P_{mid} is a linear interpolation between P_{hi} and P_{low},

$$P_{mid} = P_{low} + (P_{hi} - P_{low})\frac{SOC - 54.75}{55.25 - 54.75} \tag{15}$$

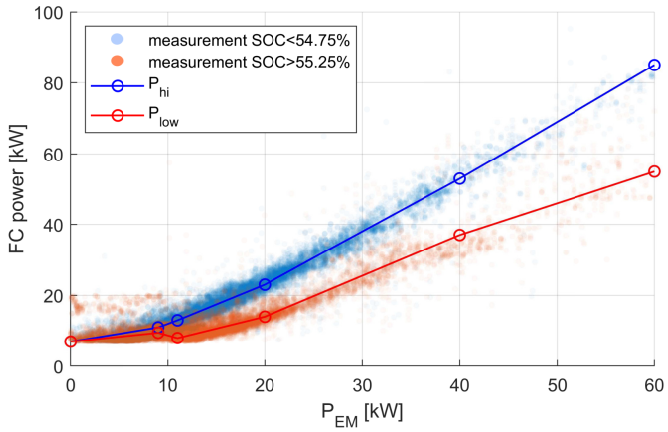

Figure 11. Power deliver by the FC as function of SOC and P_{EM}

From P^*_{FC}, the filtered power P^{fil}_{FC} is computed through a first-order low-pass filter with time constant equal to 0.17 seconds. Finally, the power assigned to the FC has to be constrained according to the maximum/minimum power variation allowed. Considering the constraints presented in section II-F, the power assigned to the FC (in kW) results:

$$\begin{aligned} P_{FC}(k) = \max\{\min\{P^{fil}_{FC}(k), ... \\ P_{FC}(k-1) + 100\ t_s\}, ... \\ P_{FC}(k-1) - 100\ t_s\}. \end{aligned} \tag{16}$$

The simulation time step t_s was chosen in 0.1 seconds to be aligned with the experimental data, whose sampling rate is 10Hz. In the last two equations some variables depend on P_{EM} and SOC. This dependency was omitted in the writing of the equations for reasons of simplicity.

B. Optimal Strategy

This section presents the formulation of the global optimization problem and a known method to solve it. Reported literature shows that in the case of FCHV with active state-dependent constraints, the optimal strategy can only be found by solving the global optimization problem [5], [32], [40]. The objective of calculating the optimal strategy is to evaluate the room for improvement of Toyota Mirai EMS.

The solution to the global optimization problem consists of finding the sequence of control input $u(k), k = 1, ..., N$, that minimizes the cost function

$$\begin{aligned} J = \sum_{k=1}^{N-1} \frac{\dot{m}_{H_2}(u(k), k)}{\dot{m}^{max}_{H_2}} + \\ \alpha\ \frac{\mid I_{BAT}(\boldsymbol{x}(k), u(k), k) \mid \sigma(\boldsymbol{x}(k), u(k), k)}{I^{max}_{BAT}\ \sigma^{max}} + \\ \beta\ \frac{\mid \Delta P_{FC}(\boldsymbol{x}(k), u(k)) \mid\ \mathbb{1}(\Delta P_{FC}(\boldsymbol{x}(k), u(k)))}{\Delta P^{max}_{FC}} \end{aligned} \tag{17}$$

subject to,

$$\boldsymbol{x}(k+1) = \mathbf{f}(\boldsymbol{x}(k), u(k), k), \tag{18}$$
$$\boldsymbol{x}(1) = \boldsymbol{x_0}, \tag{19}$$
$$\boldsymbol{x}(N) = \boldsymbol{x_f}, \tag{20}$$
$$0 \leq u(k) \leq 114, \tag{21}$$
$$-30 \leq P_{BAT}(k) \leq 30, \tag{22}$$
$$45 \leq SOC(k) \leq 65, \tag{23}$$
$$-100 \leq \Delta P_{FC}(\boldsymbol{x}(k), u(k)) \leq 100, \tag{24}$$

where, $u(k) := P_{FC}(k)$ is the control input, $\boldsymbol{x}(k) := [SOC(k), I^*_{BAT}(k), x_{FC}(k)]$ the state vector, and $\mathbf{f}$ is the dynamics of the system defined by (3)-(5)-(13). The first term of the summation accounts for fuel consumption, while the second and third account for the demand of the battery and the FC, respectively. The objectives are normalized using $\dot{m}^{max}_{H_2}$, I^{max}_{BAT}, σ^{max} and ΔP^{max}_{FC}. The maximum instantaneous hydrogen consumption ($\dot{m}^{max}_{H_2}$) is 1.422 g/s, while the maximum power variation (ΔP^{max}_{FC}) is 100 kW/s. In the battery, I^{max}_{BAT} and σ^{max} are $100A$ and 2 respectively, based on the maximum currents observed from the experimental data in cycles UDDS and WLTP (Test ID 61712053 and 61712046). Weighting factors α and β allow to vary the optimal strategy performance. With α and β equal to zero, the strategy only focuses on fuel economy, whereas if α and/or β are non-zero, the strategy simultaneously minimizes fuel consumption and the demand on the battery and FC. $\mathbb{1}$ is an indicator function that equals 1 if $\mid \Delta P_{FC} \mid > 10\ kW/s$, otherwise equals 0.

Equation (20) represents the boundary conditions applied to the state variables at the end of the cycle. In this case, x_{FC} and I^*_{BAT} are free while SOC is constrained. The SOC boundary conditions are necessary to perform fair comparisons between different optimal strategies. Dynamic programming method was adopted to solve this optimization problem. This method

Table II
H_2 CONSUMPTION (IN GRAMS): MEASURED BY ARGONNE LABORATORY [12] VS. COMPUTED WITH THE PROPOSED POWERTRAIN MODEL

	Measured	Simulation
UDDS	86.4	87.2 (+0.9%)
WLTP	190.3	188.8 (-0.8%)

guarantees to find the optimal solution even in presence of active state-dependent constraints [41]. To reduce the computational time required by dynamic programming when dealing with an optimization problem with three state variables, a vectorized instead of scalar implementation was chosen. Some guidelines for this can be found in [42].

IV. SIMULATION RESULTS

This section presents the validation of both powertrain model and rule-based strategy, and the comparison between the performance of Toyota Mirai EMS and optimal strategies.

A. Validation of powertrain model and rule-based strategy

The validation of the powertrain model was performed using the cycles UDDS and WLTP. Experimental data corresponds to the last two tests mentioned in Table I. It should be noted that these tests were not used until now. For this validation is not necessary to compute the EMS as P_{FC} is directly obtained from experimental data. The evolution of the SOC are compared in Fig. 12 and the H_2 consumptions are presented in Table II.

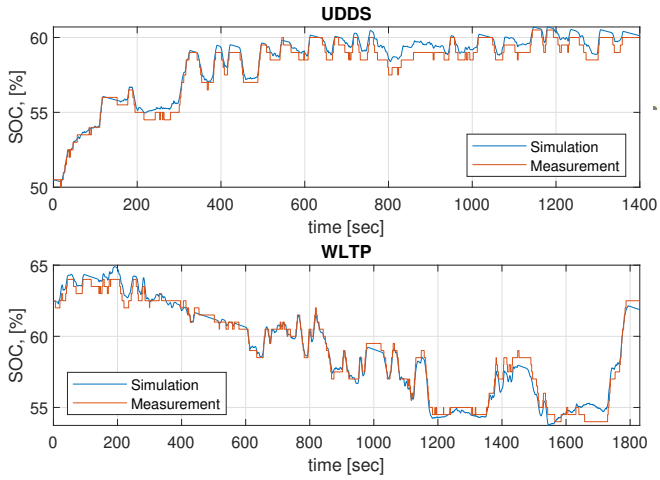

Figure 12. Validation of the powertrain model: evolution of the SOC in the battery. Measurements and inputs for simulation are taken from Test ID 61712053 and 61712046, Table I.

The differences between simulations and measurements are lower than 1% in fuel consumption and root-mean-square error in SOC is 0.46% and 0.47% in the UDDS and WLTP, respectively.

The same cycles and experimental data were used to validate the proposed rule-based strategy. Two simulations were performed per cycle: one using P_{FC} from data (Toyota Mirai strategy) and the other with P_{FC} computed by the proposed strategy. Notice that P_{FC} is updated at each time step. The comparison between the strategies is presented in terms of: energy delivered by the FC E_{FC}; H_2 consumption m_{H_2}; number of switching in the FC from idle to active $N_{switching}$; the time FC is idle t_{idle}; average of the variation of power in the FC $\overline{\Delta P}_{FC}$ (see section II-D); effective Ah-throughput in the battery Ah_{eff} (see section II-C); and state of charge of the battery at the end of the cycle SOC_{end}. Table III summarizes the results and Fig. 13 compares the P_{FC} profiles. These results show a high degree of correlation between the proposed strategy and Toyota Mirai EMS.

Table III
SIMULATION RESULTS, TOYOTA MIRAI STRATEGY VS. PROPOSED RULE-BASED STRATEGY.

Cycle		Toyota Mirai strategy	Proposed strategy
UDDS	E_{FC} [MJ]	6.64	6.68(+0.6%)
	m_{H2} [g]	87.2	88.0 (+0.9%)
	$\overline{\Delta P}_{FC}$ [kW/s]	17.4	17.4 (0%)
	$N_{switching}$ [-]	54	52 (-3.7%)
	$\%t_{idle}$ [%]	51.9	52.8 (+0.9%)
	Ah_{eff} [Ah]	4.09	3.93 (-3.9%)
	SOC_{end} [%]	60.1	60.8 (+0.7%)
WLTP	E_{FC} [MJ]	14.1	14.1 (-0.0%)
	m_{H_2} [g]	188.8	188.5 (-0.2%)
	$\overline{\Delta P}_{FC}$ [kW/s]	16.6	17.0 (+2.4%)
	$N_{switching}$ [-]	53	56 (+5.7%)
	$\%t_{idle}$ [s]	48.3%	47.1% (+1.2%)
	Ah_{eff} [Ah]	6.03	6.02 (-0.2%)
	SOC_{end} [%]	61.9	61.7 (-0.2%)

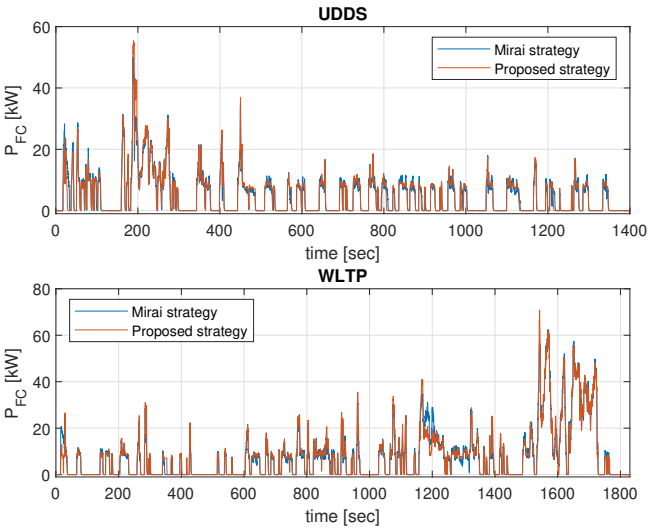

Figure 13. Comparison of the P_{FC} computed by the proposed strategy with the measurements from experimental data. Measurements and inputs for simulation are taken from Test ID 61712053 and 61712046, Table I.

B. Comparison of Toyota Mirai strategy with optimal strategies

In this section, Toyota Mirai EMS is compared with three optimal strategies obtained offline via dynamic programming. The comparison is presented in terms of fuel consumption and the demand of the FC and the battery. For the FC, the

variation of power $\overline{\Delta P}_{FC}$, idle time t_{idle} and the number of switching from idle to active $N_{switching}$ are computed; while for the battery the demand is evaluated through the effective *Ah-throughput* Ah_{eff}. The simulations performed in this section use the powertrain model presented in this work. Note that to compute the performance of Toyota Mirai EMS, the FC power (P_{FC}) was directly taken from the experimental data, so the proposed rule-based strategy is not involved in this section. The simulation results correspond to the WLTP cycle, Test ID 61712046 (Table I).

Different optimal strategies can be computed depending on the values adopted for α and β in expression (17). When $\alpha = 0$ and $\beta = 0$, the optimal strategy achieves the absolute minimum fuel consumption. This strategy will be called "Optimal Strategy 1". Fig. 14 shows the comparison between Optimal Strategy 1 and Toyota Mirai strategy.

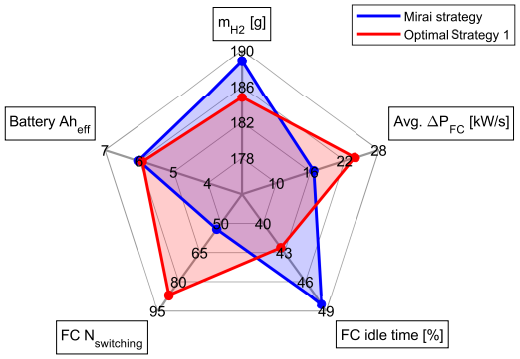

Figure 14. Mirai strategy vs. Optimal Strategy 1 ($\alpha = 0$ and $\beta = 0$).

As can be seen, the Optimal Strategy 1 achieves a savings of 2.1% of H_2 with similar demand of the battery. However, this strategy is more demanding on the FC with more switching from idle to active and higher average variation of power. To reduce the demand on the FC, a second optimal strategy was computed with $\beta = 0.352$. This strategy named "Optimal Strategy 2" is compared with Toyota Mirai strategy in Fig. 15. Optimal Strategy 2 is less demanding on the FC than Toyota Mirai strategy in terms of $\overline{\Delta P}_{FC}$ and t_{idle}, preserving 1.7% savings in H_2 consumption. The number of switching is significantly lower than the previous optimal strategy, but still above Toyota Mirai strategy. Notice that $\overline{\Delta P}_{FC} = 10kW/s$ is the lowest demand possible in the FC according to the formulation presented (see Eq. 17).

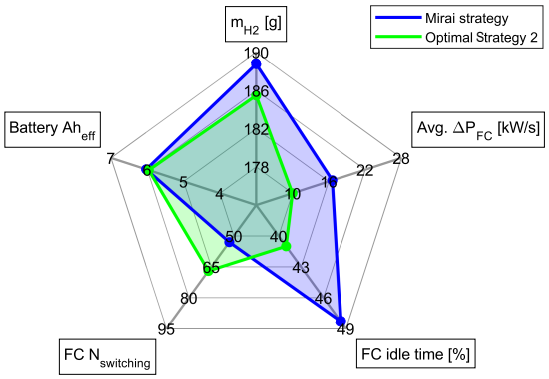

Figure 15. Mirai strategy vs. Optimal Strategy 2 ($\alpha = 0$ and $\beta = 0.352$).

So far, the demand of the battery in terms of *Ah-throughput* shows similar values between the strategies presented. It is possible to reduce the demand on the battery to the minimum by setting $\alpha = 0.563$. This strategy named "Optimal Strategy 3" is presented in Fig. 16. Its performance achieves 17% less demand on the battery, preserving 1.4% savings in H_2 consumption compared to Toyota Mirai strategy. It should also be noted the negative effect of Optimal Strategy 3 in the demand of the FC.

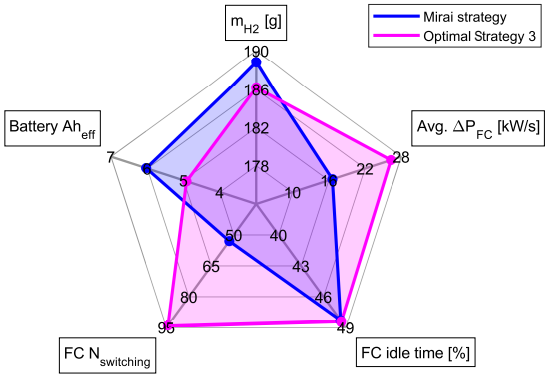

Figure 16. Mirai strategy vs. Optimal Strategy 3 ($\alpha = 0.563$ and $\beta = 0$).

It is worth noticing that a further reduction in the demand of the battery is not possible as regenerative braking is not controlled by the EMS in this formulation. It means that the energy recovered during braking and stored in the battery, has to be used at some point during the cycle to meet the SOC constraint at the end of the cycle (see Eq. 20).

Table IV summarizes the results presented so far in this section. On the other hand, Fig. 17 compares the different strategies in terms of the power profile in the FC and the evolution of the SOC throughout the cycles.

In terms of multi-objective optimization, the optimal solutions presented in this section not only belong to the Pareto frontier but also are extremes of the frontier. This means that it is not possible to obtain an optimal solution with lower H_2 consumption than Optimal Strategy 1; or lower FC power

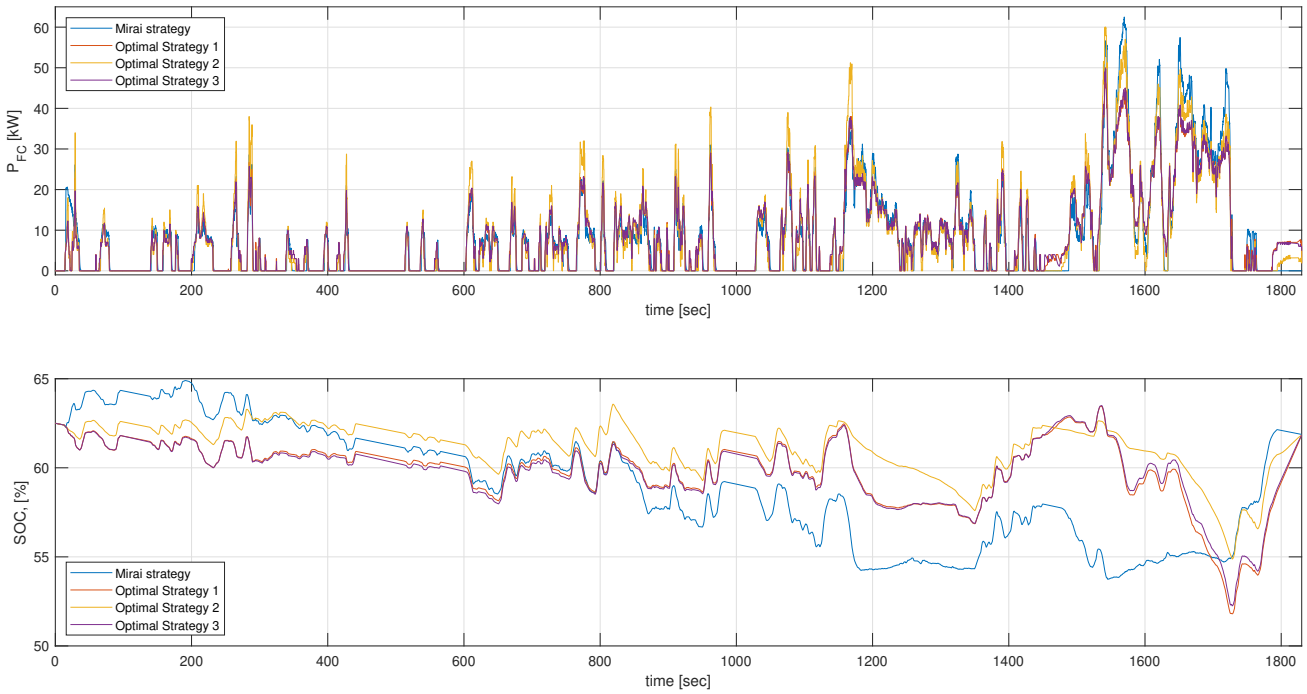

Figure 17. Mirai strategy vs. optimal strategies in terms of FC power and SOC.

variation than Optimal Strategy 2; or lower current through the battery than Optimal Strategy 3. Adopting weighting factors (α and β) within the range presented conducts to obtain intermediate optimal solutions to the solutions presented.

Table IV
SIMULATION RESULTS, TOYOTA MIRAI STRATEGY (FROM DATA) VS. DIFFERENT OPTIMAL STRATEGIES

	Toyota Mirai	Optimal Strategy 1	Optimal Strategy 2	Optimal Strategy 3
m_{H_2} [g]	188.8	**184.8**	185.5	186.2
$\overline{\Delta P}_{FC}$ [kW/s]	16.6	23.8	**10.0**	26.3
$N_{switching}$ [-]	53	87	67	94
$\%t_{idle}$ [%]	48.3	42.5	41.0	48.4
Ah_{eff} [Ah]	6.03	5.92	5.96	**4.92**

V. CONCLUSION

This work presented a low-order model of Toyota Mirai powertrain which was parameterized using experimental data. The correlation observed between the simulations and the real tests indicates that the proposed model is suitable for system level and energy management simulations. At this point it is necessary to point out a certain weakness of this work in relation to the dispersion observed in some figures. It was also presented a rule-based strategy aimed to reproduce the behavior of Toyota Mirai EMS. Simulation results showed small differences with the experimental data which indicates a good correlation between the proposed strategy and Toyota Mirai EMS.

Finally, three optimal offline EMS were computed using dynamic programming and their performances were compared with Toyota Mirai EMS. Results show that Toyota Mirai strategy achieves a H_2 consumption remarkably close to the absolute minimum obtained with Optimal Strategy 1, leaving only a 2.1% of room for improvement. Regarding the demand on the FC and the battery, it was shown that the Optimal strategies 2 and 3 are able to significantly reduce the high variations of power in the FC and the Ah-throughput in the battery, respectively. In both cases, the H_2 consumption remained close to the absolute minimum. This would have a positive effect on the FC and battery lifetime with a low impact on H_2 consumption.

REFERENCES

[1] N Sulaiman, MA Hannan, Azah Mohamed, Pin Jern Ker, EH Majlan, and WR Wan Daud. Optimization of energy management system for fuel-cell hybrid electric vehicles: Issues and recommendations. *Applied energy*, 228:2061–2079, 2018.

[2] Stephan Strahl, Noemí Gasamans, Jordi Llorca, and Attila Husar. Experimental analysis of a degraded open-cathode pem fuel cell stack. *International journal of hydrogen energy*, 39(10):5378–5387, 2014.

[3] Rod Borup, Jeremy Meyers, Bryan Pivovar, Yu Seung Kim, Rangachary Mukundan, Nancy Garland, Deborah Myers, Mahlon Wilson, Fernando Garzon, David Wood, et al. Scientific aspects of polymer electrolyte fuel cell durability and degradation. *Chemical reviews*, 107(10):3904–3951, 2007.

[4] Masanobu Uchimura and Shyam S Kocha. The impact of cycle profile on PEMFC durability. *ECS Transactions*, 11(1):1215–1226, 2007.

[5] Mauro Carignano, Vicente Roda, Ramon Costa-Castelló, Luis Valiño, Antonio Lozano, and Félix Barreras. Assessment of energy management in a fuel cell/battery hybrid vehicle. *IEEE access*, 7:16110–16122, 2019.

[6] Mark A Delucchi and Timothy E Lipman. Lifetime cost of battery, fuel-cell, and plug-in hybrid electric vehicles. *Electric and Hybrid Vehicles: Power Sources, Models, Sustainability, Infrastructure and the Market. Amsterdam, The Netherlands*, pages 19–60, 2010.

[7] Salman Habib, Muhammad Mansoor Khan, Farukh Abbas, Lei Sang, Muhammad Umair Shahid, and Houjun Tang. A comprehensive study of implemented international standards, technical challenges, impacts and prospects for electric vehicles. *IEEE Access*, 2018.

[8] Yasuhiro Nonobe. Development of the fuel cell vehicle mirai. *IEEJ Transactions on Electrical and Electronic Engineering*, 12(1):5–9, 2017.

[9] Toshihiko Yoshida and Koichi Kojima. Toyota mirai fuel cell vehicle and progress toward a future hydrogen society. *The Electrochemical Society Interface*, 24(2):45, 2015.

[10] Yoshikazu Tanaka. Development of the mirai fuel cell vehicle. In *Hydrogen Energy Engineering*, pages 461–475. Springer, 2016.

[11] Takahiko Hasegawa, Hiroyuki Imanishi, Mitsuhiro Nada, and Yoshihiro Ikogi. Development of the fuel cell system in the mirai fcv. Technical report, SAE Technical Paper, 2016.

[12] Henning Lohse-Busch, Kevin Stutenberg, Michael Duoba, and Simeon Iliev. Technology assessment of a fuel cell vehicle: 2017 toyota mirai. Technical report, Argonne National Lab.(ANL), Argonne, IL (United States), 2018.

[13] Mirai Toyota Europe. Outline of the mirai. https://www.toyota-europe.com/download/cms/euen/Toyota%20Mirai%20FCV_Posters_LR_tcm-11-564265.pdf. Accessed: 2021-03-01.

[14] Downloadable Dynamometer Database. https://www.anl.gov/es/energy-systems-d3-2016-toyota-mirai. Accessed: 2022-05-30.

[15] Olivier Tremblay and Louis-A Dessaint. Experimental validation of a battery dynamic model for ev applications. *World Electric Vehicle Journal*, 3(1):1–10, 2009.

[16] Javier Martin Cabello, Eric Bru, Xavier Roboam, Fabien Lacressonniere, and Sergio Junco. Battery dynamic model improvement with parameters estimation and experimental validation. *IMAACA*, September 2015.

[17] Mingyue Zhang and Xiaobin Fan. Review on the state of charge estimation methods for electric vehicle battery. *World Electric Vehicle Journal*, 11(1):23, 2020.

[18] Lorenzo Serrao, Zakaria Chehab, Y Guezennee, and Giorgio Rizzoni. An aging model of ni-mh batteries for hybrid electric vehicles. In *Vehicle power and propulsion, 2005 IEEE conference*, pages 8–pp. IEEE, 2005.

[19] Lorenzo Serrao, Simona Onori, Giorgio Rizzoni, and Yann Guezennec. A novel model-based algorithm for battery prognosis. *IFAC Proceedings Volumes*, 42(8):923–928, 2009.

[20] Vincenzo Marano, Simona Onori, Yann Guezennec, Giorgio Rizzoni, and Nullo Madella. Lithium-ion batteries life estimation for plug-in hybrid electric vehicles. In *Vehicle Power and Propulsion Conference, 2009. VPPC'09. IEEE*, pages 536–543. IEEE, 2009.

[21] A Di Filippi, S Stockar, S Onori, M Canova, and Y Guezennec. Model-based life estimation of li-ion batteries in phevs using large scale vehicle simulations: An introductory study. In *Vehicle Power and Propulsion Conference (VPPC), 2010 IEEE*, pages 1–6. IEEE, 2010.

[22] Lorenzo Serrao, Simona Onori, Antonio Sciarretta, Yann Guezennec, and Giorgio Rizzoni. Optimal energy management of hybrid electric vehicles including battery aging. In *Proceedings of the 2011 American control conference*, pages 2125–2130. IEEE, 2011.

[23] Frano Barbir. *PEM fuel cells: theory and practice*. Academic Press, 2012.

[24] Paganelli Rodatz, G Paganelli, A Sciarretta, and L Guzzella. Optimal power management of an experimental fuel cell/supercapacitor-powered hybrid vehicle. *Control Engineering Practice*, 13(1):41–53, 2005.

[25] Diego Hernán Feroldi et al. Control and design of pem fuel cell-based systems. 2009.

[26] Chun-Yan Li and Guo-Ping Liu. Optimal fuzzy power control and management of fuel cell/battery hybrid vehicles. *Journal of power sources*, 192(2):525–533, 2009.

[27] Francisco Soriano Alfonso et al. A study of hybrid powertrains and predictive algorithms applied to energy management in refuse-collecting vehicles. *Materia (s)*, 22:05–2015, 2015.

[28] Luis Valverde, Carlos Bordons, and Felipe Rosa. Integration of fuel cell technologies in renewable-energy-based microgrids optimizing operational costs and durability. *IEEE Transactions on Industrial Electronics*, 63(1):167–177, 2016.

[29] D. Feroldi, M. Serra, and J. Riera. Energy management strategies based on efficiency map for fuel cell hybrid vehicles. *Journal of Power Sources*, 190(2):387–401, 2009.

[30] Javier Solano Martinez, Daniel Hissel, Marie-Cécile Pera, and Michel Amiet. Practical control structure and energy management of a testbed hybrid electric vehicle. *IEEE Transactions on Vehicular Technology*, 60(9):4139–4152, 2011.

[31] Souleman Njoya Motapon, Louis-A Dessaint, and Kamal Al-Haddad. A comparative study of energy management schemes for a fuel-cell hybrid emergency power system of more-electric aircraft. *IEEE Transactions on Industrial Electronics*, 61(3):1320–1334, 2014.

[32] Diego Feroldi and Mauro Carignano. Sizing for fuel cell/supercapacitor hybrid vehicles based on stochastic driving cycles. *Applied Energy*, 183:645–658, 2016.

[33] Pablo García, Juan P Torreglosa, Luis M Fernández, and Francisco Jurado. Control strategies for high-power electric vehicles powered by hydrogen fuel cell, battery and supercapacitor. *Expert Systems with Applications*, 40(12):4791–4804, 2013.

[34] M Uzunoglu and MS Alam. Modeling and analysis of an fc/uc hybrid vehicular power system using a novel-wavelet-based load sharing algorithm. *IEEE Transactions on Energy Conversion*, 23(1):263–272, 2008.

[35] Zhihong Yu, Donald Zinger, and Anima Bose. An innovative optimal power allocation strategy for fuel cell, battery and supercapacitor hybrid electric vehicle. *Journal of Power Sources*, 196(4):2351–2359, 2011.

[36] Vanessa Paladini, Teresa Donateo, Arturo De Risi, and Domenico Laforgia. Super-capacitors fuel-cell hybrid electric vehicle optimization and control strategy development. *Energy Conversion and Management*, 48(11):3001–3008, 2007.

[37] Sousso Kelouwani, Kodjo Agbossou, Yves Dubé, and Loïc Boulon. Fuel cell plug-in hybrid electric vehicle anticipatory and real-time blended-mode energy management for battery life preservation. *Journal of Power Sources*, 221:406–418, 2013.

[38] Hong Huo, Hao Cai, Qiang Zhang, Fei Liu, and Kebin He. Life-cycle assessment of greenhouse gas and air emissions of electric vehicles: A comparison between china and the us. *Atmospheric Environment*, 108:107–116, 2015.

[39] Yoshinobu Hasuka, Hiroyuki Sekine, Koji Katano, and Yasuhiro Nonobe. Development of boost converter for mirai. Technical report, SAE Technical Paper, 2015.

[40] Mauro G Carignano, Ramon Costa-Castelló, Vicente Roda, Norberto M Nigro, Sergio Junco, and Diego Feroldi. Energy management strategy for fuel cell-supercapacitor hybrid vehicles based on prediction of energy demand. *Journal of Power Sources*, 360:419–433, 2017.

[41] Donald E Kirk. *Optimal control theory: an introduction*. Courier Corporation, 2012.

[42] Mauro G. Carignano, Norberto M. Nigro, and Sergio Junco. HEVs with reconfigurable architecture: a novel design and optimal energy management. In *Integrated Modeling and Analysis in Applied Control and Automation (IMAACA), 2016 I3M*, pages 59–67, 2016.

ACKNOWLEDGMENTS

This work is part of the project MAFALDA (PID2021-126001OB-C31) funded by MCIN/ AEI /10.13039/501100011033 and by "ERDF A way of making Europe", and also part of the project MASHED (TED2021-129927B-I00) funded by MCIN/ AEI/10.13039/501100011033 and by the European Union Next GenerationEU/PRTR.